Advancing corrosion protection in confined spaces: a solvent-free UV LED-curable coating for steel pipelines with enhanced barrier properties and harsh environment performance

Alessandro Condini (ID)**, Carlo Trentalange, Angela Giuliani, Andrea Cristoforetti, Stefano Rossi**

Abstract This study investigates a novel solvent-free, UV LED-curable coating as a robust corrosion protection solution for the inner surface of steel pipelines. The properties of the UV-cured film were characterized in terms of reactivity, thermomechanical properties, and adhesion to metal substrates. The coating was applied to the inside steel pipelines and cured using a patented UV LED lamp designed to fit in confined spaces. Finally, electrochemical impedance spectroscopy characterization and an accelerated cyclic electrochemical technique were performed on the coated pipes to study the corrosion protection properties of the coating, both with and without the addition of inorganic fillers. The results were compared to a commercially available thermally cured coating. It was found that the UV-cured coating confers high barrier properties, effectively preventing liquid penetration even under elevated temperature conditions. Furthermore, the corrosion protection performance in harsh environments was comparable to and, in some cases, higher than standard epoxy linings.

Keywords Coatings, UV LED, Photopolymers, Corrosion protection, Electrochemical impedance spectroscopy

A. Condini (✉), A. Cristoforetti, S. Rossi
Department of Industrial Engineering, University of Trento, Trento, Italy
e-mail: alessandro.condini-1@unitn.it; a.condini@elixe.com

A. Condini, C. Trentalange, A. Giuliani
Elixe srl, Trento, Italy

Introduction

Corrosion is responsible for catastrophic damage to the infrastructures of oil industries, devices, and other establishments.[1–3]

Applying paints and coatings is one of the most convenient and promising methods to face corrosion. Currently, environmental concerns have grown significantly with the use of traditional coatings, particularly regarding (a) the release of volatile organic compounds (VOCs) and hazardous air pollutants (HAPs), which pose health and toxicity risks, and (b) the high energy demand associated with the coating's application processes.[4,5]

In response to these environmental challenges, radiation-curable coatings have emerged as an attractive alternative to conventional thermal-curing coatings. These entirely solvent-free coatings offer the distinct advantage of not requiring high-temperature application but only exposure to specific wavelengths of UV radiation to cure.[6] Two different UV light sources can be used to radiate and cure UV curable coatings: UV pressure lamps (usually medium pressure) and UV light emitting diode (LED) lamps.

UV pressure lamps are polychromatic light sources containing mercury or noble gases. They can emit a broad multiple-line spectrum from 200 to 400 nm. Since they emit a broad multiple-line spectrum, the large amount of radiation is only helpful if the photoinitiator (PI) absorbs these distinct wavelengths.[7,8] Furthermore, a significant part of the energy is wasted as heat, and an efficient air-cooled system is required to avoid undesirable effects during the polymerization reaction, such as the thermal degradation of the polymer to be cured.[7,8]

On the other hand, the UV LEDs are monochromatic light sources available at different wavelengths. Thus, the light emitted has a relatively narrow wavelength range, which can be tailored for a particular PI.

Since they emit a very narrow wavelength range, no infrared radiation is emitted; thus, overheating does not occur, resulting in the long lifetime of the diode (10,000–20,000 h). Moreover, since the energy consumption is lower than that of UV pressure lamps, they can be used with a battery power supply. Thus, small mobile devices have been developed and are available on the market. For these reasons, they are also used when UV-curing coatings are applied directly in the field.

This technology presents several advantages: (a) low capital cost; (b) shallow energy requirement for crosslinking at room temperatures; (c) avoidance of solvent emissions; and (d) the ability to guarantee similar corrosion protection performance as traditional thermal curing coatings.[7]

Over the past years, UV technology has gained several successes in many fields, especially wood coatings, plastic coatings, printing inks, electronics, adhesives, and metal coatings. However, UV technology in protective metal coatings fields currently needs more application. In the field of anticorrosive coatings for heavy industry, it represents a new frontier to be explored. In 2019, only 2% of the UV technology market was addressed to the metal protection field application.[9]

A UV-curable coating consists of (a) multifunctional oligomers, (b) reactive diluent (reactive monomers), and (c) photoinitiators (PI). The first generation of UV-curable coatings system was made of unsaturated resin and benzoic acid, which was developed by Bayer Company in 1968.[10]

Due to their high functionality, multifunctional oligomers provide a high degree of crosslinking to the coatings. For the curable system induced by the free radicals, such as the UV curable coatings here presented, the frequently used monomers include the unsaturated polyester, epoxy acrylate (EA), polyurethane acrylate (PUA), polyester acrylate resin, polyether acrylate resin and so on.[10,11] The radical polymerization mechanism is a chain mechanism consisting of an initiation, propagation, and termination step. In the initiation phase, reactive radical species are generated by the decomposition of the PI molecule catalyzed by ultraviolet light. These radicals are very reactive and trigger the opening of the C=C double bond of the acrylate group, thus starting the propagation of the polymer chain.[10]

The reported study focuses on preventing corrosion of pipes used to transport or produce oil, gas, water, and chemical substances by applying a UV-curable coating. Pipe corrosion can involve the external wall of the pipe or the internal wall pipe. Generally, internal pipeline corrosion can occur only in the presence of corrosive agents such as water or other aqueous compounds; carbon dioxide (CO_2) for the formation of dilute organic or inorganic acids; or sulfur for the formation of acids or growth of bacteria. The corrosive agents continue the corrosion until they have been removed or consumed in the corrosion reactions.

Common approaches to prevent inner pipe corrosion are (a) dehydration, (b) inhibitors, (c) protective coatings, (d) buffering, (e) cleaning pigs, and (f) biocide application.[12–14] Protective coating application can provide a smooth surface, reducing drag and improving the flow of the transported fluid. It is the most used approach applied in the oil and gas fields because it can ensure a uniform protective barrier on the pipe's inner surface.[15]

Scientific literature reports several studies about novel protective coatings for metal structures based on UV-curable coatings.[1,6,16–18] However, only a few studies about the effects of fillers' particles on UV coating features have been reported. Fillers allow the coating to achieve increased durability or reduce film thickness at consistent mechanical performance. The minerals are also less expensive than the resin; filling some volumes results in a more cost-effective product.[19] Mineral fillers play an essential role in the corrosion protection effectiveness of a coating; however, they can compromise the successful occurrence of the UV curing reaction. Thus, their kind and concentration selection are pivotal.

Deflorian and Fedel[20] reported on a study about improving UV coatings' corrosion protection using montmorillonite nanoparticles. Using electrochemical impedance spectroscopy (EIS), they analyzed the corrosion behavior of three different UV coatings: (a) UV-curable waterborne urethane acrylic coatings, (b) modified montmorillonite nanoparticles in UV-cured epoxy coatings, and (c) a combination of the sol-gel route with UV curable moieties in urethane acrylic coatings. Through their analysis, they found that nanoparticles dramatically affected the corrosion protection properties of the UV-cured coatings.

In the end, even if several studies investigate the corrosion protection performance of UV-curable coating, only some are investigating their performance in real applications. Legros et al.[21] published a patent reporting their invention of a UV-curable internal resistance reduction coating for steel pipes and application/curing equipment. The equipment reported, suitable for pipes with internal diameter (ID) > 50 cm, consisted of two UV lamps mounted onto a rail. Due to the dimensions of UV bulbs and their fragility, the equipment described in the patent was claimed to be optimal for pipes with an ID of about 100 cm and 12 m long.

Over the definition of an optimal corrosion protection UV-curable coating formulation, a significant issue of UV-curable coatings' application to the inner wall of pipes is the curing process because the UV light source must be brought inside the pipe to allow successful coating curing.

Condini et al.[22] have recently reported a novel UV LED light source designed and developed to bring the UV light inside pipes and provide efficient and uniform irradiation respecting the dimensional constraints due to the dimensional features of the entry hole of the tubes used for pipes having an ID < 20 cm. Condini

et al. developed a UV LED lamp torch with a 360° radiation emission pattern to cure UV curable coatings in difficult-to-reach surfaces such as the inner surface of pipelines. In particular, the UV LED light source was designed to fit inside pipes with diameters ranging from 40 to 200 mm, the most common dimensions of pipes used in the oil and gas downhole.

In the present study, the prevention of corrosion of the internal wall of pipes by applying a novel UV-curable coating has been investigated. The new UV-curable coating presented here, RAD03, has been formulated by replacing the epoxy novolac thermal curing resin used in the thermal curing coating used as the benchmark, reported as NG coating, with an epoxy-acrylate UV curing resin, and keeping the filler composition unchanged. NG coating is currently applied to protect the inner surface of the pipes used for oil extraction. This strategy evaluates the resin replacement effect on the coatings' corrosive properties, even considering the fillers' role.

The UV LED light source proposed by Condini et al.[22] has been used to cure the samples of UV-curable coating investigated in this study and applied on the internal surface of steel pipes. The radiation wavelength of 395 nm was selected to crosslink the UV-curable coatings.

The corrosion protection performance of RAD03 has been compared with the corrosion protection performance of NG coating, investigating the effect of the presence of the fillers into the coatings and the role played by the resin, evaluating the corrosion protection performance of their relatives without fillers VRAD03 and VNG. The corrosion protection features of the UV coating have been investigated using EIS at different temperatures and accelerated cyclic electrochemical technique (ACET) at room temperature. The electrochemical characterization has been functional in knowing the corrosion protection mechanism involved when the coatings undergo thermal and marine corrosion stress.

Experimental procedure

Materials

The specimens of UV curing coatings are called VRAD03 and RAD03 (ELIXE, Trento, Italy), and the reference thermal curing coatings are VNG and NG (ELIXE, Trento, Italy). All the coatings specimens have been prepared in the ELIXE chemical laboratory. The general coating formulations are reported in Table 1 because the detailed coating formulations are companies' properties and are confidential information.

Steel substrates used for coating application consisted of API 5 CT steel with an inner diameter of 62 mm and wall thickness of 5.5 mm, employed as a standard in the oil and gas industry for oil wells. The

chemical composition of API 5 CT steel consists of 0.34–0.39 carbon, 0.20–0.35 silicon, 1.25–1.50 manganese, 0.020 phosphorous, 0.015 sulfur, 0.15 copper, 0.20 chromium, 0.20 nickel, and 0.020 aluminum. Before application, each pipe's internal surface was sandblasted according to ISO 8501-1 to achieve a 2½–3 cleanliness standard, having a roughness average of 65 μm.

Thermally cured and UV-cured coatings were formulated and tested with an inorganic fillers' mixture of quartz, talc, and TiO_2 in fixed concentration, whose specific concentration is withheld due to a confidentiality agreement with the paint supplier. The weight percentage of fillers used in the thermal formulation was given as critical pigment volume concentration (CPVC). CPVC represents the transition point above or below which substantial differences in the appearance and behavior of paint films will be encountered. It is that point in a pigment-vehicle system at which just sufficient binder is present to fill the voids left between the pigment particles incorporated in the film after volatilization of thinner. It represents the densest degree of packing of the pigment particles commensurate with the degree of dispersion of the system.[23] CPVC of the thermal formulation was defined during the research and development activities of ELIXE laboratories using several corrosion protection tests on a bibliography of formulations with different filler content. The selected thermal formulation was also tested on the field six months before the market placement.

In contrast, concentration in UV formulation was determined after a series of tests as maximum concentration allowed to obtain a fully cured film of 100 μm thickness after exposure to 380 mW/cm² for 60 s. A bibliography of UV-coating formulations with different fillers' concentrations has been prepared to evaluate which one might be optimal for successful curing and corrosive protection effectiveness through performance tests in the laboratory. RAD03 fillers' concentration higher than 40% w/w hinders the complete curing of a 100 μm coating layer with detrimental effects on mechanical and protective coating performance.

Table 1 provides the definition and general composition of the four formulations.

LED lamps and coating preparation

This study employed two LED lamps with similar intensity output but different geometries. The first was a DROLED L76 flat static LED lamp (Photo Electronics srl, Italy) with 395 nm wavelength, flat window optics, and a maximum intensity of 7 W/cm²; this lamp was used to cure samples on flat substrates. The second lamp consisted of 120 1W LEDs with 395 nm wavelength mounted on six arrays around a water-cooled body. The shape and dimension of this lamp allowed for a uniform cure of the coating applied on the inside

Table 1: General composition of the four formulations used

Coating			Composition (g)			
Name	Curing type	Epoxy	Amine (%)	Solvents	Additives	Fillers
VNG	T	25	55[1]	13.0	2.5	0
NG	T	25	55[1]	13.0	2.5	58.5

Coating			Composition (g)			
Name	Curing type	Epoxy acrylate	Diluent	Photoinitiator	Additives	Fillers
VRAD03	UV	34	20.5	2	3.5	0
RAD03	UV	34	20.5	2	3.5	40

[1]Amine curing agent used in wt% to the concentration of epoxides
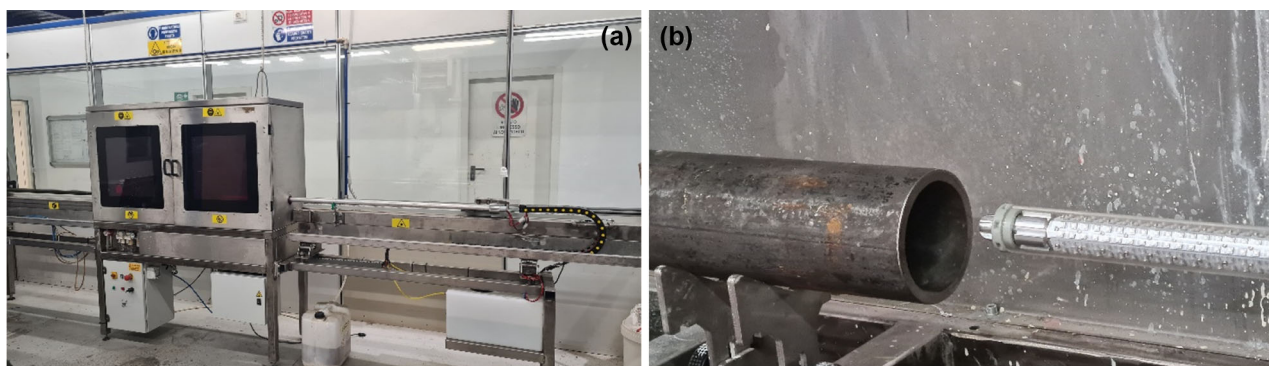
Fig. 1: Picture of (a) coating application and curing equipment and (b) UV light source (patent pending)

of the steel pipes used in this project. The irradiation pattern of this lamp and its dependence on the distance from the substrate surface is illustrated in a previous study published by our team.[22] Both lamps were used at a set distance, allowing a total intensity of 380 mW/cm^2 for a total exposure of 120 s.

Coating application on the inside of pipes was performed using a rotary atomizer capable of dispersing the paint formulation continuously and with reasonable control of wet film thickness. For pipes, a coating consisting of 2 layers of 100 μm dry film thickness each was applied to emulate the process application. Thermal paint was cured in the oven at 100°C for 2 h, while UV coating was cured using the cylindrical LED for a total exposure of 120 s per layer. The final thickness was measured with a digital gauge, resulting in a value of 195 ± 8 μm. Pictures of the application, curing equipment, and the light source are shown in Fig. 1.

Characterization

Fourier Transform Infrared Spectroscopy

Fourier transform infrared spectroscopy (FTIR) was performed using a Thermo Scientific Nicolet iS 50 Spectrometer (Thermo Fisher Scientific, Waltham, Massachusetts, USA) operating in transmission. Each measurement was an average of 32 spectra collected in the spectral range from 4000 to 600 cm^{-1} with a resolution of 4 cm^{-1}. Uncured samples were deposited on a silica wafer using a 12 μm hand coater; a spectrum was collected before and after exposure to an LED lamp with an intensity of 380 mW/cm^2 for 120 s. Three different measurements were collected for each formulation, and the spectra collected were processed using the software OMNIC spectra. The conversion was calculated by comparing the peak areas corresponding to the reactive group in the formulation before and after the curing process. By monitoring their decrease over time, it was possible to calculate the degree of conversion (α) using the following equation:

$$\propto (t) = 1 - \frac{(A_{Et})(A_{R0})}{(A_{E0})(A_{Rt})} \tag{1}$$

where α is the conversion percentage at time t, A_{E0} and A_{Et} are the areas of the reactive group peak at time 0 and time t, respectively, while A_{R0} and A_{Rt} are the areas of the reference peak at time 0 and time t, respectively. The reference peak for each formulation corresponded to a signal not changing during the reaction.

Dynamic mechanical thermal analysis

Dynamical mechanical thermal analysis (DMTA) was used to evaluate glass transition temperature and viscoelastic properties of resin mixtures as a function of temperature. A Tritec 2000 DMA equipment from Triton Technology Ltd. was used with a temperature ramp of 3°C/min, a frequency of 1 Hz, and a total displacement of 20 μm. RAD03 and VRAD03 samples comprising 100 and 120 μm thickness were polymerized on polypropylene (PP) substrates using a static LED lamp with an intensity of 380 mW/cm^2 for 120 s for RAD03 and VRAD03. The samples of NG and VNG coating were cured onto PP substrates in an oven at 80°C for 120 min. Glass transition temperatures (T_g) presented are the average of at least two experiments for each sample.

Adhesion measurements

Adhesion tests of resin formulations were performed according to ISO 4624—pull-off test using flat blasted steel samples measuring 100 x 40 x 10 mm. Samples with two thickness layers of 100 and 120 μm were polymerized on the steel substrates using a static LED lamp with an intensity of 380 mW/cm^2 for 120 s. An Elcometer 510 automatic pull-off adhesion gauge with a pull rate of 1 MPa/s was used to measure adhesion strength. The pull piece consisted of a 20 mm aluminum dolly glued to the substrate's surface using a bicomponent epoxy adhesive (Scotch-Weld DP 460). Dollies were cured for 3 h at 50°C before the test. Each measurement was performed at least four times for each coating, and the resulting average was presented as the final value.

Electrochemical characterization

All electrochemical characterization tests were performed using the PalmsSens4 potentiostat (PalmsSens, Houten, Netherlands). The electrochemical cell (Fig. 2) consisted of a coated pipe section with an end glued to a polymethylmethacrylate (PMMA) base. The inside of the pipe was then filled with an electrolyte solution of 3.5 wt% NaCl to simulate a corrosive working environment. The total area exposed to 3.5 wt% NaCl was constant and equal to 168 cm^2. An Ag/AgCl electrode was used as a reference electrode (RE) to apply a controlled voltage across the coating, and a platinum wire acted as the counter electrode (CE). These two electrodes were immersed in the 3.5 wt% NaCl, while the working electrode (WE) was the pipe itself, and the system was used to measure the resulting current in the coating. All measurements were performed, placing the electrochemical cell inside a Faraday cage to provide better isolation and avoid interferences to the system.

Fig. 2: The electrochemical cell

Two methods were used to characterize the coating electrochemically: electrochemical impedance spectroscopy (EIS) and accelerated cyclic electrochemical technique (ACET).

In the EIS method (ISO 16773), the coating impedance was measured as the AC voltage applied at the reference electrode divided by the resulting AC measured at the counter electrode. The impedance value was used to indicate the coating's barrier properties. For this study, the EIS tests were carried over a scanning frequency range from 0.01 to 10^5 Hz and an amplitude of 0.015 V over the open circuit potential (OCP). EIS measurements were performed for each sample at increasing temperatures from room to 90°C using steps of 10°C. The samples were taken in the oven for 30 min to ensure the homogeneous heating of the 3.5 wt% NaCl solution and the pipe section. To avoid the evaporation of the 3.5% NaCl solution, the pipe was covered. During the EIS experiment, the sample was placed onto a heater to keep the temperature of the electrochemical cell, and the temperature was constantly controlled using a thermocouple.

The ACET method was performed according to ISO 17463, and it was used to determine the coating adhesion to the metal substrate and its resistance to degradation. It consisted of an initial EIS performed with the same parameters already described. It was followed by a cathodic polarization in which a constant voltage of − 4.0 V was applied for 20 min and a relaxation period of 3 h without voltage. The steps described were repeated for a total of six cycles. The software used for the data manipulation was PSTrace 5.9; each measurement was performed on two separate
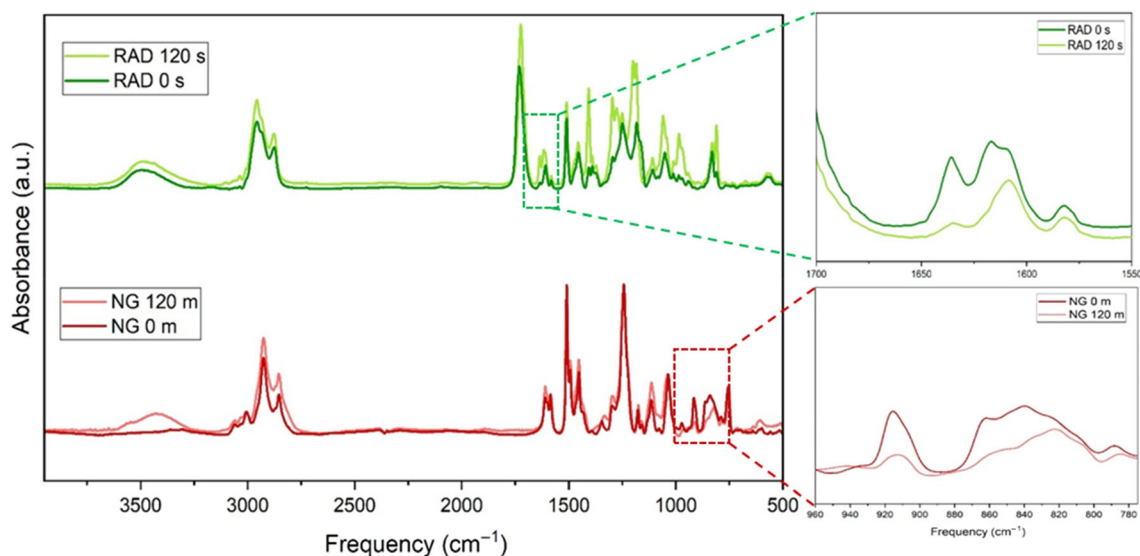
Fig. 3: FTIR spectra of VRAD03 and VNG formulations before and after curing

samples. If the results were similar, only the data from one sample was used for the plots.

Results

Crosslinked film properties

Conversion

The curing process of the two formulations was evaluated by measuring the relative concentration of their respective functional groups before and after the reaction. Figure 3 reports the FTIR spectra of the two formulations before and after irradiation. For the thermally cured epoxy reference coating, the distinctive peaks are the stretching of the C–O bond of the oxirane functionality at 915 cm^{-1} and the stretching of the C–O–C ring at 831 cm^{-1}. Here, the signal at 915 cm^{-1} was used because it was more easily readable. Another signal that can be used to confirm the ongoing reaction is the strengthening of the signal at 3500 cm^{-1} relative to the stretching of the –OH group. The formation of more hydroxyl groups directly affects the oxirane group ring opening reaction. Differently, the response in the radical formulation can be followed by looking at the disappearance of the peak at 1635 cm^{-1}, which can be ascribed to the C=C double bond of the acrylate function, which reacts after UV exposure. The aromatic ring C=C double bond stretch peaks at 1610 cm^{-1} and the C–O bond stretch at 1510 cm^{-1} were used as reference peaks for the epoxy-based and acrylate base coating, respectively. The conversion degrees ($\propto$) after 120 s of curing of RAD03 and NG coatings were found by applying equation (1) to the absorbance data of the FTIR spectra obtained before and after curing. RAD03 showed a $\propto$ value of

0.7 while NG revealed a $\propto$ value of 0.6. These values are lower than the conversion values calculated for VNG and VRAD03, respectively 0.7 and 0.8. The decrease in the conversion degree can be ascribed to the different concentrations of fillers inside the coatings. The higher concentration of fillers in NG coating hinders the curing reaction, bringing it to a lower $\propto$.[24]

Viscoelastic properties

Dynamic mechanical thermal analysis (DMTA) was used to determine the viscoelastic properties of the four coatings samples as a function of increasing temperature. The storage modulus (E') has been used to determine stiffness, filler/matrix interfacial bonding, and degree of crosslinking, as reported in Fig. 4a. The material's glass transition temperature (T_g) is the maximum value of the tan delta curve, as reported in Fig. 4b.

Figure 4 can be used to evaluate the effect of the two curing approaches investigated, thermal and UV irradiation, and the impact of adding the fillers to the pure resins.

In the E' (Pa) vs T (°C) graph, three different regions can be identified: glassy region, transition region, and rubbery plateau.[25] In the glassy region, the components of the composite result in a very compact state, like they were frozen, and E' shows higher values.[26] Increasing temperature E' decreases for all the coating samples because the resins become increasingly fluid and finally soft upon the glass transition occurring and reaching the rubbery plateau. Generally, the thermal curing samples VNG and NG reveal the highest value of E' in the glassy region, suggesting higher stiffness than the coating samples obtained by UV irradiation curing, VRAD03, and
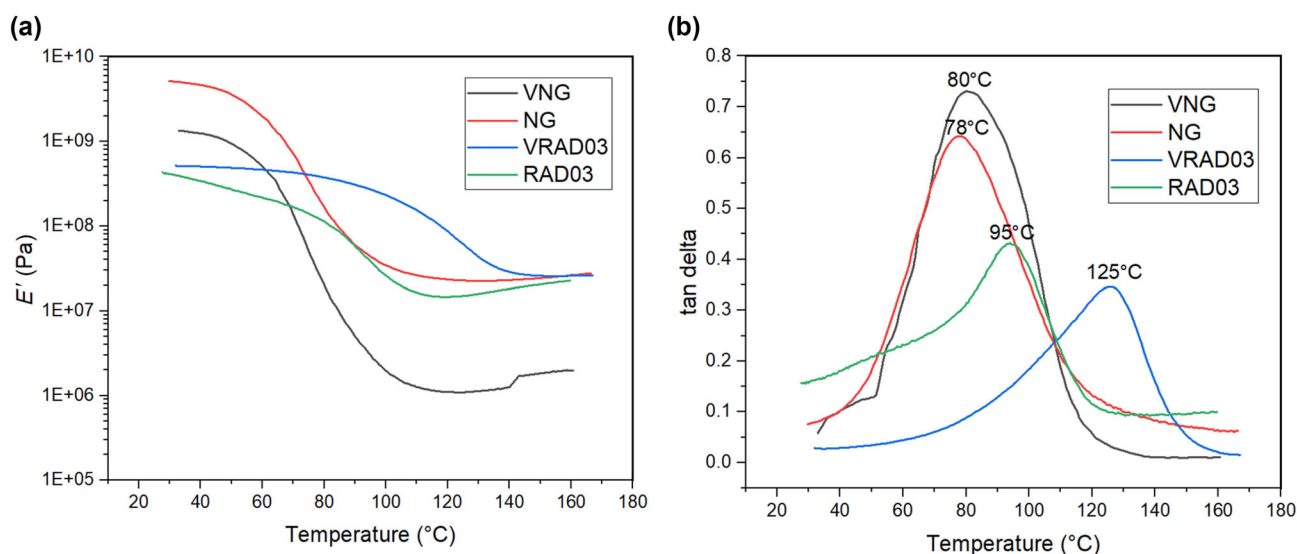
Fig. 4: (a) Storage modulus and (b) tan delta curves in the function of temperature obtained from DMTA measures of VNG (black), NG (red), RAD03 (green), and VRAD03 (blue) (Color figure online)

RAD03. The difference in stiffness between thermal-cured and UV-cured samples could be ascribed to the unreacted resin inside VRAD03 and RAD03 layers due to the scattering effect of the fillers' particles, which limits UV light penetration, hindering the resin curing.

Finally, as shown in Fig. 4b, VNG and NG coating samples show tan delta peak values higher than VRAD03 and RAD03, indicating a higher degree of molecular mobility than VRAD03 and RAD03 samples. These latter appear broader due to the nonhomogeneity of crosslinking density inside the coatings' layers, likely due to different polymer chain lengths in the case of broad polydispersity. The wide shape of the storage modulus curves in Fig. 4a supports this behavior.[25–27]

Concerning the effect of fillers addition to the resin, as reported in Table 2, the reduction of the E_r can be observed for the UV-cured formulations, from 2.9×10^7 Pa of VRAD03 to 1.7×10^7 Pa of RAD03. The reduction of the modulus can be ascribed to the hindering of the curing process of the polymer matrix due to the presence of fillers, as supported by the noticeable decrease of T_g, going from 125°C for the VRAD03 formula to 95°C for RAD03. This effect arises from the scattering effect of the fillers' particles, which limits UV light penetration inside the polymeric matrix during the curing process and reduces the T_g of the UV-cured coating. Moreover, as suggested by the shape of the storage modulus curves (Fig. 4a) in the glass transition region, adding fillers into VRAD03 negatively affects the crystallinity of the UV-cured resin.[26] This behavior is also supported by the reduction of T_g. Inside VRAD03, more polymer chains are constrained to a greater degree at the crystal/amorphous interface and require higher temperatures to

Table 2: DMTA measures reporting glass transition temperature (T_g) and modulus at rubbery plateau (E_r) for each of the four coatings

Coating	Glass transition T (°C)	E_r (Pa)
VNG	80	1.1 e06
NG	78	2.7 e07
VRAD03	125	2.9 e07
RAD03	95	1.7 e07

mobilize, resulting in the increased transition temperature.[27]

As reported in Table 2, T_g of VNG coating measured with DMTA is not significantly affected by adding fillers to obtain the NG sample. Indeed, it varies from 80°C for VNG to 78°C in NG. The effect of the fillers can be observed in the increase of E_r from 1.1×106 Pa of VNG to 2.7×107 Pa of NG. This finding can be ascribed to strong interactions between fillers and epoxy matrix that make NG stiffer than VNG.[25]

Adhesion

Adhesion tests for the four coating specimens were performed right after curing and after immersion in HCl 20% solution for three days at ambient temperature and pressure (25°C and 1 atm) to simulate the aggressive environment of oil and gas wells.[5,13] The standard used to evaluate this test is a common practice of coating suppliers in the oil and gas sector in Europe and Asia: the minimum initial pull-off adhesion of 10 MPa[5] is required for a coating to be

Table 3: Pull-off adhesion data obtained for RAD03 with fillers, RAD03 without fillers, and NG coatings pristine after immersion in 20% HCl solution

Coating	Adhesion pristine (MPa)	HCl @ 20% three days (MPa)	Adhesion loss (%)
VRAD03	16.60 ± 0.50 (SE)	10.30 ± 1.50 (62%)	38 (adhesive failure)
RAD03	25.00 ± 0.00 (SE)	14.91 ± 0.64 (60%)	40 (cohesive failure)
VNG	16.80 ± 2.26 (SE)	8.15 ± 0.54 (49%)	51 (adhesive failure)
NG	20.21 ± 0.66 (SE)	10.35 ± 4.00 (51%)	49 (cohesive failure)
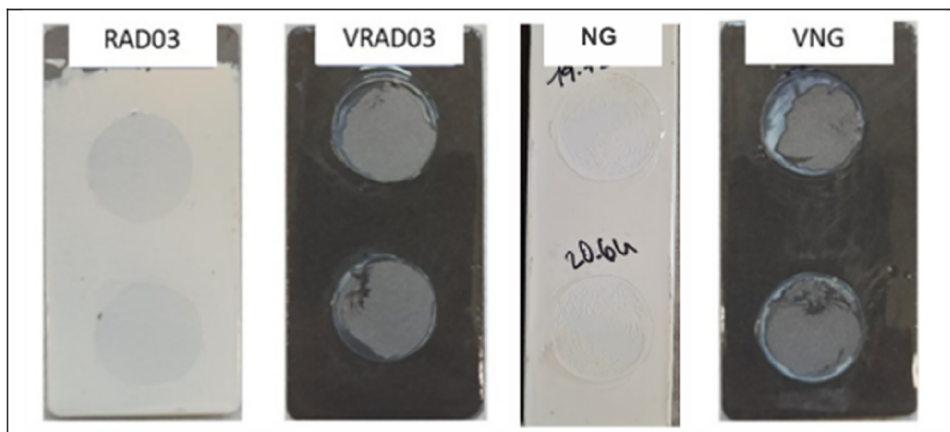
Fig. 5: Picture of the pull-off test adhesion of NG, VNG, RAD03, and VRAD03

considered suitable for metal protection. The adhesion cannot decrease over 50% of the adhesion value of the right prepared specimen (adhesion pristine), which is considered ideal for the test after acid immersion (indicated in brackets in Table 3).

As shown in Table 3, the adhesion of both thermal and UV-cured coatings improves significantly after filler addition. At first sight, although the retention of an adhesion higher than 10 MPa is required by the quality standard applied by ELIXE srl, all the samples, UV and thermal cured, showed a reduction of adhesion upon immersion in 20% HCl solution.

RAD03 and NG coatings revealed a cohesive failure, while VRAD03 and VNG coatings had an adhesive failure. The adhesive failure of VRAD03 and VNG has been ascribed to interaction forces between the polymer chains greater than those generated between polymer molecules and the metal substrate. Cohesive failure of the coatings can be addressed by the swelling of the coating by absorption of the 20% HCl solution or degradation reactions of the resins, such as the epoxy ring opening reaction.[28]

Further, NG adhesion is higher than VNG adhesion, 20.21 MPa and 16.80 MPa, respectively. RAD03 has an adhesion of 25.00 MPa, which is the upper limit of the instrument used, meaning that the coating does not break from the substrate. As expected, VRAD03 has an adhesion of 16.60 MPa, lower than RAD03, because of the filler's absence. The increasing adhesion conferred by the filler can be explained by the effect the

inorganic particles have on the crack propagation inside the polymeric matrix: fillers create bridges across the initial forming cracks, hindering delamination.[29] After HCl immersion, RAD03, both filled and unfilled, also shows a more excellent adhesion compared to the tests performed in standard conditions, with 62% of initial adhesion for the unfilled version and 60% for the filled one respectively, and overall higher than 10.00 MPa.

Figure 5 shows pictures of the pull-off test adhesion samples.

Electrochemical properties

Electrochemical impedance spectroscopy (EIS)

Figure 6 shows the electrochemical impedance spectroscopy results on the four different coatings. The impedance modulus $|Z|$ generally decreases with increasing temperature for all the coatings as their mechanical properties are influenced by the combined effect of heat and electrolyte penetration. This has an impact on the corrosion protection of the coating and is the cause of its behavior to change from mainly capacitive to mainly resistive. When the coating behaves primarily as a capacitor, only charge and discharge processes occur at the interface of the WE and the electrolyte; no electrochemical reactions occur because the diffusion of the electrolyte through the
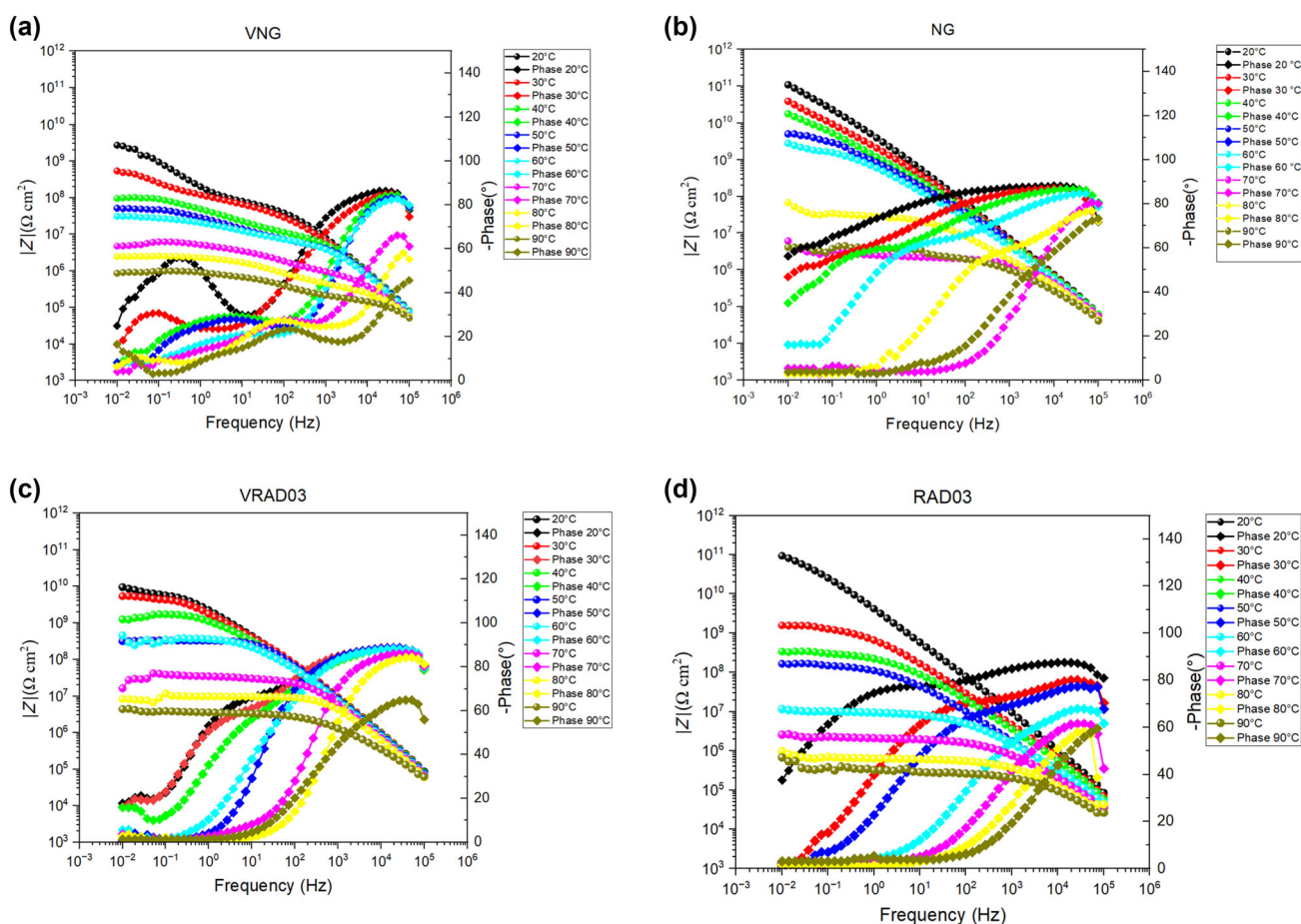
Fig. 6: EIS Bode plots of VNG (a), NG (b), VRAD03 (c), and RAD03 (d) taken at different temperatures

coating network is hindered by its barrier properties microstructure. In this case, the Bode plot of the coating is a straight line with a slope of -1,[30] as can be seen on the low-temperature EIS curves of the NG coating in Fig. 6b and RAD03 in Fig. 6d.

On the other hand, when the electrolyte starts to penetrate inside the polymer microstructure, the coating begins to swell due to electrolyte absorption. It has less capacitive behavior, facilitating the possibility of electrochemical reactions on the metal surface. In this case, the $|Z|$ curves show a plateau at low frequencies, and the coating behaves less as a capacitor. This behavior can be observed in the coatings specimens formulated without fillers VNG and VRAD03 in the temperature range studied, starting from 20 to 90°C, respectively Fig. 6a and 6c. As expected, VNG and VRAD03 do not contain fillers; thus, they cannot hinder electrolyte permeation even at low temperatures.

While in RAD03, the behavior change occurs at 30°C; NG coating shows the change at 50°C. For RAD03 and NG coating, the permeation of electrolytes inside the coating layer starts when heating stress affects the viscoelastic properties of the coating, bringing a change of the microstructure and, of course,

a change of the barrier properties. Even if the filler species and their relative concentration are the same, for both RAD03 and NG, the total amount of concentration of fillers in RAD03 is lower than in NG coating; for this reason, the change of behavior in RAD03 occurs first, then in NG coating.

Moreover, as demonstrated from the T_g data achieved by DMTA, the faster electrochemical behavior change of RAD03 can be ascribed to a less uniform crosslinking of the resin matrix due to the scattering of the UV curing light of the filler particles, resulting in a RAD03 T_g lower of 30°C than the one obtained for VRAD03. The poor crosslinking uniformity of RAD03 even explains the electrochemical behavior difference to NG coating, for which, as supported by their T_g values, the crosslinking occurs with negligible difference by its relative without fillers, VNG.

Generally, the higher the coating's impedance at low frequencies at a defined temperature, the higher its barrier properties and corrosion protection; a coating is considered to have good corrosion protection if its impedance measured at low frequencies is higher than $106 \ \Omega \ cm^2$.[30–33]

On this basis, all the tested coatings demonstrated excellent corrosion protection behavior at room tem-
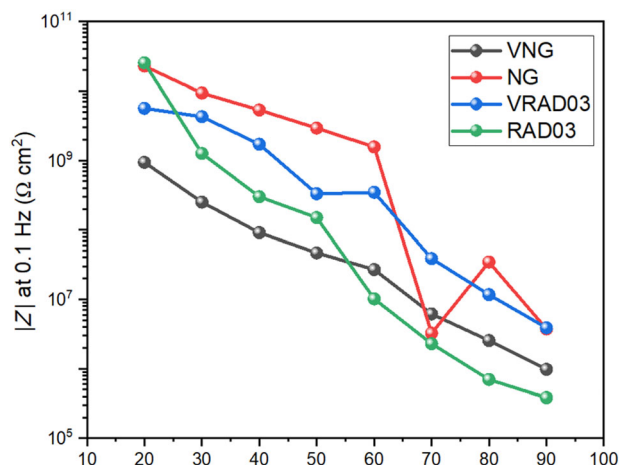
Fig. 7: Comparison of the |Z| collected at 0.1 Hz in the function of temperature obtained for VNG, NG, VRAD03, and RAD03

perature as their impedance at low frequency is between 9.5×10^8 and 2×10^{10} Ω cm^2. Figure 7 |Z| at 0.1 Hz is plotted as a function of temperature for each coating. Increasing temperature, the impedance varies differently for the different coatings. The coatings formulated without VNG and VRAD03 fillers show |Z| values at 0.1 Hz lower than their relatives' containing fillers. The lower |Z| values for VNG and VRAD03 can be ascribed to the absence of fillers facilitating the electrolyte permeation inside the coating layer. VRAD03 shows |Z| values higher than VNG in the temperature range between 20 and 40°C, likely due to the different curing technology. Solvents in VNG can create defective points when solvents evaporate during the curing process.

|Z| decrease in the function of temperature for VRAD03 occurs slower than RAD03, despite the absence of fillers. This behavior, at first counterintuitive, can be explained by the fact that fillers do increase the barrier properties of the UV-curable coating, as can be seen by the increase of |Z| at room temperature from VRAD03 to RAD03. However, they also decrease the overall crosslinking density by lowering the light penetration through the coating and consequently reducing glass transition temperature (T_g), as seen in Table 2.

Despite RAD03 at 20°C showing |Z| higher than NG, it decreases steeply, increasing the temperature: at 30°C, the |Z| of RAD03 reaches 1.3×10^9 Ω cm^2. |Z| decrease for NG coating is slower than RAD03; it reaches 1.6×10^9 Ω cm^2, heating up to 60°C. The different rates of |Z| for RAD03 and NG coatings can be due to the different concentrations of fillers inside the coatings: RAD03 contains almost 20% of fillers less than NG, allowing a less efficient barrier when temperature increase facilitates electrolyte permeation process inside the coating layer.

In the end, from the |Z| profiles plotted in the function of the temperature, each coating has a critical

Table 4: Summary of T_g wet found for each coating sample

Sample	Wet T_g (°C)
NG	41
VNG	40
RAD03	38
VRAD03	48

temperature at which a change of slope occurs. Li et al.[34] suggested that the temperature at which the change of slope occurred is the temperature T_g of the aqueous electrolyte plasticized film, and therefore, lower than the dry film T_g measured by DSC. This temperature can be named "wet T_g" and represents the temperature at which the capacitive coating behavior turns into a resistive due to a more favorable water absorption into the coating.[5]

At temperatures higher than the wet T_g, the coatings undergo a swelling phenomenon due to electrolyte absorption, which consequently has a detrimental effect on their microstructure. This negatively affects their corrosion performance, as the decrease of |Z| suggests.

As can be seen, the wet T_g values found by EIS measuring (Table 4) do not agree with the results found by DMTA analysis.

VRAD03 shows a higher temperature when DMTA and EIS are measured. RAD03, as measured by DMTA, shows a temperature lower than VRAD03 but not higher than NG and VNG; it could be likely due to the use of the optimal concentration of fillers to achieve a fully cured film of 100 μm thickness after exposure to 380 mW/cm^2 for 60 s, which is different from the application of the CPVC as done for the NG coating formulation.

Thus, the trend obtained by DMTA analysis:

$$VRAD03 > RAD03 > NG > VNG \qquad (2)$$

has changed in the following, as achieved by EIS analysis:

$$VRAD03 > NG > VNG > RAD03 \qquad (3)$$

Accelerated cyclic electrochemical techniques (ACET)

ACET method is usually applied to quickly evaluate protection performance when the coating is subjected to marine conditions.[35–37] During the ACET test, the coating is stressed by applying a cathodic polarization at − 4 V. The cathodic polarization drives two different processes into the coating layer:

- the absorption and migration of electrolyte cations such as H$^+$ and Na$^+$ through the coating due to the
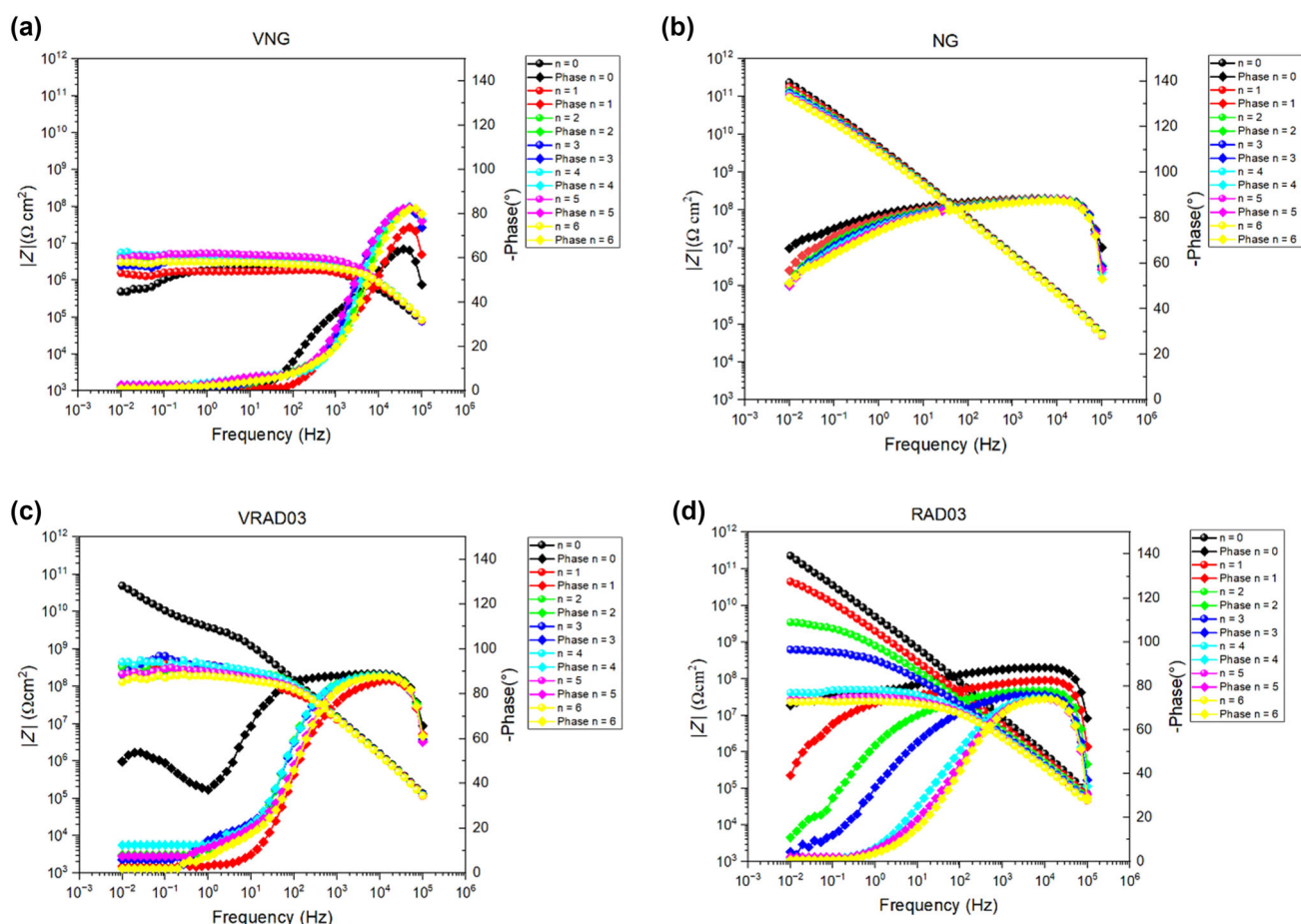
Fig. 8: ACET Bode and Nyquist plots of VNG (a), NG (b), VRAD03 (c), and RAD03 (d)

negative potential imposed at the metallic substrate surface. The concentration of positive charges in the coating must be neutralized by entering anions such as OH^- and Cl^-. The passage of ions (which can also be hydrated) through the coating can cause its deterioration and the formation of pores.[35]

- the water reduction occurs at a potential more negative than about -1.2 V vs. calomel electrode, leading to H_2 gas evolution onto the metallic surface. The cathodic reaction is the following:

$$2H_2O + 2e^- \rightarrow H_2 + 2OH^- \qquad (4)$$
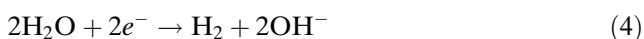
The water reduction will occur first if the electrolyte passes through the coating and reaches the interface. The evolution of H_2 increases local delamination, giving rise to the failure of the coating system that is reflected in the impedance variation.[38]

The successful occurrence of these two processes depends on the coating properties such as permeability to ions, adhesion to the substrate, local film delamination, susceptibility of the coating to form cracks because of its high rigidity, and, of course, the cathodic potential applied. Figure 8 reports the ACET Bode

plots of NG coating, VNG, RAD03, and VRAD03. The measurement indicated as $n = 0$ is the measurement acquired before the first polarization.

The reference coating, NG coating, has shown excellent corrosion protection even after seven cycles at -4 V cathodic polarization and subsequent relaxation. Its Bode plot (Fig. 8b) shows negligible difference in impedance between the consecutive cycles, which is stable around 1×10^{11} Ω cm^2. Thus, the migration of electrolyte ions into the NG coating layers and the occurrence of water reduction reaction at the metal surface is hindered by its microstructure, which is made by the stacking of the fillers present in the coating. The importance of the filler is highlighted by the Bode plot of VNG coating samples (Fig. 8a). The VNG paint has poorer protection performance than NG coating with fillers. The impedance value remains around 1×10^7 Ω cm^2 during the ACET cycles, showing a negligible decrease. The electrochemical behavior of VNG coating is also different, as VNG has a less capacitive behavior. It agrees with the poorer corrosion protection performance due to the absence of fillers that can create a passive barrier and a more tortuous path for the electrolyte ion's migration through the coating layers. Thus, the lack of fillers in
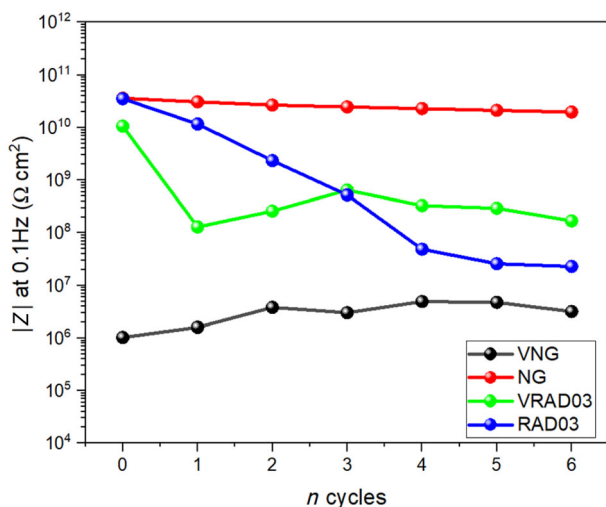
Fig. 9: Comparison of the |Z| collected at 0.1 Hz in the function of the number of cycles obtained for VNG, NG, VRAD03, and RAD03

VNG favors the ion's absorption and migration process.

The Bode plot of RAD03 is reported in Fig. 8d. The Bode plot of RAD03 coating shows an impedance decrease from 2.6×10^{11} to $2.3 \times 10^7 \; \Omega \; cm^2$ during the test. After the fourth cycle, the impedance has a negligible reduction and remains fixed around $2.3 \times 10^7 \; \Omega \; cm^2$. It turns less performant after the second cycle of the experiment, suggesting a coating feature change upon the second cathodic polarization application. No blistering has been observed on the coating sample during the experiment. The Bode plot revealed only one process occurring, which could be related to ion absorption and migration inside the coating. The change in RAD03 behavior with fillers can be due to the shift in permeability to ions and coating surface porosity due to the cathodic polarization during the test.

In the end, Fig. 8c shows the Bode plot of VRAD03. The shows a change in its electrochemical behavior upon the first cathodic polarization cycle. The faster-turning behavior of VRAD03 is likely due to the absence of fillers in its formulation, which favors the ion's absorption and migration process. This hypothesis is supported by only one process in the Bode plot and the absence of coating blistering during the experiment.

For a better comprehension of the findings achieved by the ACET analysis, a plot of the |Z| profiles of each coating in the function of the number of cycles is shown in Fig. 9.

As previously reported, by comparing the |Z| profiles as a function of the number of cycles performed during the ACET analysis, |Z| decrease among the consecutive cycles for NG coating is negligible; |Z| remains set in the order of $10^8 \; \Omega \; cm^2$. On the other hand, the reduction of |Z| RAD03 occurs faster within the first three cycles, reaching a plateau upon the fourth cycle. |Z| decrease of about four orders of magnitude.

By comparing the ACET findings achieved by investigating VNG and VRAD03, it is possible to observe that VRAD03 performs better than VNG. VRAD03 has |Z| values in the order of $10^8 \; \Omega \; cm^2$, while VNG has impedance in the order of $10^6 \; \Omega \; cm^2$. This resulted in an agreement with Curtarolo et al.[6] that accelerated corrosion testing on steel has shown superior corrosion resistance can be obtained with high-performance UV coatings compared to conventional epoxy and urethane corrosion resistance coating with much higher thicknesses.

Conclusions

This study has provided valuable insights into the potential of replacing traditional thermal curing coating technology with more environmentally friendly UV curing coating technology. By investigating RAD03 and comparing its performance to the established NG coating, we have demonstrated that UV coatings can provide comparable or superior corrosion protection. RAD03 showed stronger adhesion to steel substrates, even after exposure to acidic conditions, exceeding the performance of epoxy coatings.

However, considering the electrochemical characterization at different temperatures, RAD03 coating showed a faster decrease in impedance values than NG coating, reaching an impedance value lower than $1 \times 10^8 \; \Omega \; cm^2$ at 90°C. This indicates the potential adverse effect of filler concentration on the overall barrier properties of the coating. Even after ACET analysis, it showed an impedance value lower than $1 \times 10^8 \; \Omega \; cm^2$ upon the third cycle. Although the total concentration of fillers used in RAD03 was lower than in NG coating and ensured the complete curing of a 100 μm thick layer, further consideration should be given to the optimal total concentration of fillers. As demonstrated by the T_g values achieved by the DMTA analysis, the total amount of fillers used in RAD03 has detrimental effects on the uniformity of the cross-linking resin matrix.

Indeed, VRAD03, without fillers, displayed a capacitive behavior comparable to that of the NG coating even at temperatures as high as 90°C, showing impedance values higher than $1 \times 10^8 \; \Omega \; cm^2$ and higher than the VNG coating when undergoing thermal stress, meaning higher corrosion protection. Therefore, as demonstrated in this study, pure resin UV-curable coatings, applied at the same thickness as a traditional thermal curing coating, can provide comparable protective performance. However, a pure resin UV coating would not be a cost-effective product for the market; thus, filler use is preferable, and the optimal definition of its total concentration is necessary to obtain a filled UV-curable coating with improved

protective performance than its relative without fillers and avoid possible detrimental effects during the UV curing reaction.

Ultimately, the strategy used in this study to easily convert a thermal curing coating into a UV curing coating achieved valid and exciting results, even if it should be improved in some aspects. These findings open promising avenues for future research. Subsequent studies may investigate the influence of various coating thicknesses and filler compositions on the corrosion protection behavior.

References

1. Ur Rahman, O, Kashif, M, Ahmad, S, ''Nanoferrite Dispersed Waterborne Epoxy Acrylate: Anticorrosive Nanocomposite Coating.'' *Prog. Org. Coat.*, **80** 77–86 (2015)
2. Kim, J, Lim, W, Lee, Y, Kim, S, Park, SR, Suh, SK, Moon, I, ''Development of Corrosion Control Document Database System in Crude Distillation Unit.'' *Ind. Eng. Chem.*, **50** 8272–8277 (2011)
3. Perez, TE, ''Corrosion in Oil and Gas Industry: An Increasing Challenge for Materials.'' *JOM*, **65** 1033–1042 (2013)
4. Wang, S, Ang, H, Tade, MO, ''Volatile Organic Compounds in Indoor Environment and Photocatalytic Oxidation: State of the Art.'' *Environ. Int.*, **33** 694–705 (2007)
5. Giuliani, A, Giunta, D, Condini, A, *Advancing in Liquid Coatings: High Performant Liquid Epoxy Coating for Oil Well Tubing, High Temperature and High Pressure Resistant.* ADIPEC, Abu Dhabi (2020)
6. Curtarolo, B, *UV Technology for the Protection of the Surface.* Rad Tech, Berea (2014)
7. Dreyer, C, Mildner, F, *Applications of LEDs for UV Curing.* Springer, Cham, pp. 415–434 (2016)
8. Uhl, A, Mills, RW, Vowels, RW, ''Knoop Hardness Depth Profiles and Compressive Strength of Selected Dental Composites Polymerized with Halogen and LED Light Curing Technologies.'' *J. Biomed. Mater. Res.*, **63** 729–738 (2002)
9. Engberg, D, *Market Overview 2019.* RadTech 2019, Monaco (2019)
10. Liu, F, Liu, A, Tao, W, Yang, Y, ''Preparation of UV Curable Organic/Inorganic Hybrid Coatings—A Review.'' *Prog. Org. Coat.*, **145** 105685 (2020)
11. Jung, DH, Jeong, HM, Kim, BK, ''Organic–Inorganic Chemical Hybrids Having Shape Memory Effect.'' *J. Mater. Chem.*, **20** 3458–3466 (2010)
12. Cole, IS, Marny, D, ''The Science of Pipe Corrosion: A Review of the Literature on the Corrosion of Ferrous Metals in Soils.'' *J. Corros. Sci.*, **56** (1) 5–16 (2012)
13. Brondel, D, Edwards, R, Hayman, A, Hill, D, Mehta, S, Semerad, T, ''Corrosion in the Oil Industry.'' *Oilfield Rev.*, **6** 4–18 (1994)
14. Tuttle, RN, ''Corrosion in Oil and Gas Production.'' *J. Pet. Technol.*, **39** 756–762 (1987)
15. Lyon, SB, ''Advances in Corrosion Protection by Organic Coatings: What We Know and What We Would Like to Know.'' *Prog. Org. Coat.*, **102** 2–7 (2017)
16. O'Kefee, M, Fahrenholtz, W, Curatarolo, B, ''Multifunctional UV (MUV) Curable Corrosion Coatings for Aerospace Applications.'' *Metal Finish.*, **108** 28–31 (2010)
17. Li, T, Zhang, ZP, Rong, MZ, Zhang, MQ, ''Self-healable and Thiol–ene UV-Curable Waterborne Polyurethane for Anticorrosion Coating.'' *J. Appl. Polym. Sci.*, **136** (26) 47700 (2019)
18. Jafarzadeh, S, Adhikari, A, Sundall, P, Pan, J, ''Study of PANI-MeSA Conducting Polymer Dispersed in UV-Curing Polyester Acrylate on Galvanized Steel as Corrosion Protection Coatings.'' *Prog. Org. Coat.*, **70** 108–115 (2010)
19. Preston, J, ''Impact of Extender Minerals in UV Varnish.'' *Coatings*, **11** 24–28 (2023)
20. Deflorian, F, Fedel, M, ''UV-Curable Organic Polymer Coatings for Corrosion Protection of Steel.'' In: Makhlouf, ASM (ed.) *Handbook of Smart Coatings for Material Protection*, pp. 530–559. Woodhead Publishing (2014). https://doi.org/10.1533/9780857096883.3.530
21. Legros, P, Stone, V, Gonzales, E, ''Pipes for Pipelines Having Internal Coating and Method for Applying the Coating.'' US 2015/0167706, 2015
22. Condini, A, Morozov, V, Trentalange, C, Rossi, S, ''Modeling LEDs Radiation Patterns for Curing UV Coatings Inside of Pipes.'' *Opt. Mater.*, **144** 114275 (2023)
23. Asbeck, WK, Van Loo, M, ''Critical Pigment Volume Relationships.'' *Ind. Eng. Chem.*, **41** 1470–1475 (1949)
24. Shagh, PK, Stansbury, JW, ''Role of Filler and Functional Group Conversion in the Evolution of Properties in Polymeric Dental Restoratives.'' *Dent. Mater.*, **30** 586–593 (2014)
25. Gheith, MH, Aziz, MA, Ghory, W, Saba, N, Asim, M, Jawaid, M, Alothman, O, ''Flexural, Thermal, and Dynamic Mechanical Properties of Date Palm Fibers Reinforced Epoxy Composites.'' *J. Mater. Res. Technol.*, **8** 853–860 (2019)

26. Ramli, H, Zainal, N, Hess, M, Chan, C, "Basic Principle and Good Practices of Rheology for Polymers for Teachers and Beginners." *Chem. Teach. Int.*, **4** 307–326 (2022)

27. Toft, M, "The Effect of Crystalline Morphology on the Glass Transition and Enthalpic Relaxation Poly(ether-ether-ketone)." Thesis. Department of Metallurgy and Materials, The University of Birmingham—College of Engineering and Physical Sciences. Birmingham, p. 85 (2011)

28. Verma, C, Olasunkanmi, LO, Akpan, ED, Quraishi, MA, Dagdag, O, El Gouri, M, Sherif, M, Ebenso, EE, "Epoxy Resins as Anticorrosive Polymeric Materials: A Review." *React. Funct. Polym.*, **156** 104741 (2020)

29. Wei, H, Xia, J, Zhou, W, Zhou, L, Hussain, G, Lin, Q, Ostrikov, K, "Adhesion and Cohesion of Epoxy Based Industrial Composite Coatings." *Compos. Part B Eng.*, **193** 108035 (2020)

30. Gray, GSL, Bernard, R, "EIS: Electrochemical Impedance Spectroscopy: A Tool to Predict Remaining Coating Life?" *JPCL*, **20** 66–74 (2003)

31. Noè, C, Iannucci, L, Malburet, S, Grallot, A, Sangermano, M, Grassini, S, "New UV-Curable Anticorrosion Coatings from Vegetable Oils." *Macromol. Mater. Eng.*, **306** 21000229 (2021)

32. Cristoforetti, A, Rossi, S, Deflorian, F, Fedel, M, "On the Limits of the EIS Low-Frequency Impedance Modulus as a Tool to Describe the Protection of Organic Coatings Exposed to Accelerated Aging Test." *Coatings*, **13** 598 (2023)

33. ICP Margarit-Mattos, "EIS and Organic Coatings Performance Revesting Some Key Points." *Electrochem. Acta*, **354** 136725 (2020)

34. Li, J, Jeffcoate, CS, Bierwagen, GP, Mills, DJ, Tallman, DE, "Thermal Transition Effects and Electrochemical Properties in Organic Coatings: Part 1—Initial Studies on Corrosion Protective Organic Coatings." *Corrosion*, **54** 763–771 (1998)

35. Gimeno, MJ, Puig, M, Chamorro, S, Molina, J, March, R, Oró, E, Pérez, P, Gracenea, JJ, Suay, JJ, "Improvement of the Anticorrosive Properties of an Alkyd Coating with Zinc Phosphate Pigments Assessed by NSS and ACE." *Prog. Org. Coat.*, **95** 46–53 (2016)

36. Gimeno, MJ, Chamorro, S, March, R, Oró, E, Pérez, P, Gracenea, J, Suay, J, "Anticorrosive Properties Enhancement by Means of Phosphate Pigments in an Epoxy 2k Coating. Assessment by NSS and ACET." *Prog. Org. Coat.*, **77** 2024–2030 (2014)

37. D'Elia, MF, Magni, M, Romanò, T, Trasatti, SPM, Niederberger, M, Caseri, WR, "Smart Anticorrosion Coatings Based on Poly(phenylene Methylene): An Assessment of the Intrinsic Self-Healing Behavior of the Copolymer." *Polymers*, **14** 3457 (2022)

38. Gracenea, JJ, "The Fast Lane to Failure." *Eur. Coat. J.*, **03** 84 (2011)